Eur. Phys. J. E **21**, 69–80 (2006)
DOI 10.1140/epje/i2006-10045-9

THE EUROPEAN PHYSICAL JOURNAL E

Rubber friction on smooth surfaces

B.N.J. Persson[1,a] and A.I. Volokitin[1,2]

[1] IFF, FZ-Jülich, 52425 Jülich, Germany
[2] Samara State Technical University, 443100 Samara, Russia

Received 3 July 2006 and Received in final form 19 September 2006 /
Published online: 9 November 2006 –

Abstract. We study the sliding friction for viscoelastic solids, *e.g.*, rubber, on hard flat substrate surfaces. We consider first the fluctuating shear stress inside a viscoelastic solid which results from the thermal motion of the atoms or molecules in the solid. At the nanoscale the thermal fluctuations are very strong and give rise to stress fluctuations in the MPa-range, which is similar to the depinning stresses which typically occur at solid-rubber interfaces, indicating the crucial importance of thermal fluctuations for rubber friction on smooth surfaces. We develop a detailed model which takes into account the influence of thermal fluctuations on the depinning of small contact patches (stress domains) at the rubber-substrate interface. The theory predicts that the velocity dependence of the macroscopic shear stress has a bell-shaped form, and that the low-velocity side exhibits the same temperature dependence as the bulk viscoelastic modulus, in qualitative agreement with experimental data. Finally, we discuss the influence of small-amplitude substrate roughness on rubber sliding friction.

PACS. 61.41.+e Polymers, elastomers, and plastics – 62.20.Qp Tribology and hardness – 62.40.+i Anelasticity, internal friction, stress relaxation, and mechanical resonances

1 Introduction

The friction between rubber and smooth substrate surfaces is a topic of extreme practical importance, *e.g.*, for wiper blades (in particular on hydrophobic glass), rubber O-ring seals, and in the contact region between the tire rubber and the steel rim on a wheel [1,2].

When a rubber block is sliding on a very rough substrate, such as a tire on a road surface, the friction is almost entirely due to the energy dissipation in the bulk of the rubber as a result of the fluctuating (in time and space) viscoelastic deformations of the rubber by the substrate asperities [3–5]. This mechanism becomes unimportant when the substrate is very smooth. In the limiting case of a perfectly smooth substrate, the friction is instead due to local stick-slip events at the sliding interface. Schallamach [6] has proposed a molecular mechanism for the local stick slip, see Figure 1, where a rubber polymer chain at the interface attaches to the moving countersurface, stretches, detaches, relaxes, and reattaches to the surface to repeat the cycle (similar models have been studied in Refs. [7,8]). During each cycle, the elastic energy stored in the polymer chain is dissipated as heat during the (rapid) detachment and relaxation phase, and this is assumed to be the origin of the (macroscopic) friction. This model is probably suitable to describe situations where individual molecules can bind to scarce but strong pinning sites presented on the substrate surface, *i.e.*, situations where the pinning potential is strongly corrugated. However, the Schallamach idea cannot be applied to weak pinning in a quasi-periodic potential. First, for physisorption systems the energy barriers for (vertical) detachment are usually much higher than the energy barriers for lateral sliding [9], so one would not expect any detachment to occur. Secondly, with respect to the stresses rubber materials are usually exposed to, rubber is nearly incompressible and it is not easy to imagine how single molecules strongly confined at the interface are able to switch between an elongated (stretched) state and a relaxed (curled-up) state as indicated in the figure. Furthermore, the sliding friction tends to exhibit the same temperature dependence as the bulk rubber viscoelastic modulus $E(\omega)$ as described by the

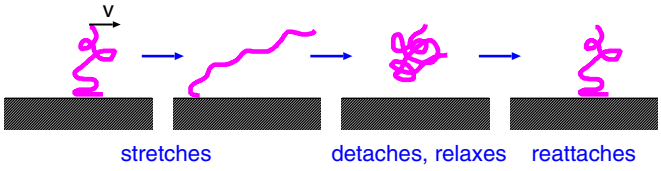

Fig. 1. The classical description of a polymer chain in contact with a lateral moving countersurface. The chain stretches, detaches, relaxes, and reattaches to the surface to repeat the cycle.

[a] e-mail: b.persson@fz-juelich.de

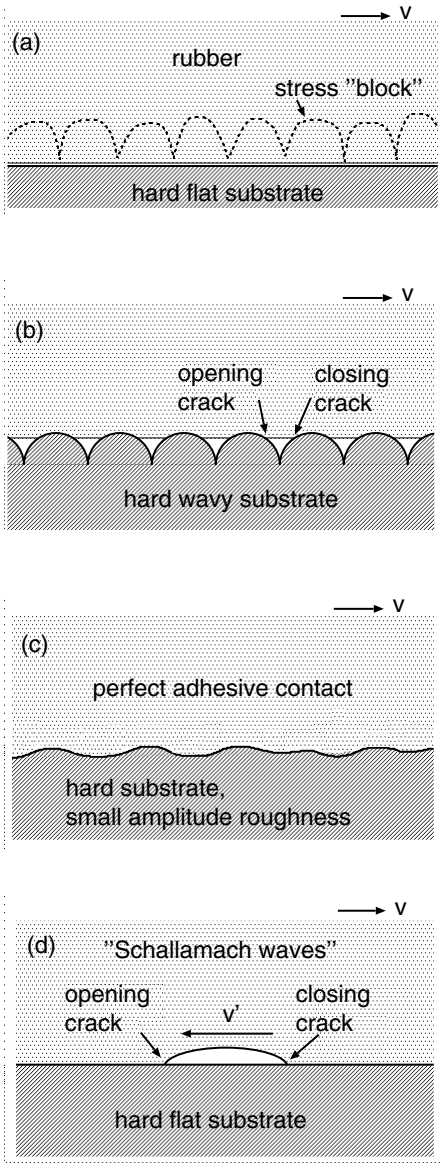

Fig. 2. Four different processes where the adhesive rubber-substrate interaction contributes to rubber friction.

Williams-Landel-Ferry (WLF) [10] shift factor a_T. This indicates the crucial role of the bulk rubber in the friction process.

We believe that the local stick-slip processes, which must occur at the sliding interface, involve relative large rubber volume elements, always in adhesive contact with the substrate. That is, during sliding, small patches (with a diameter of order $D \sim 10$–$100\,\mathrm{nm}$) or *stress domains* [11] of rubber at the sliding interface perform stick-slip motion: during stick the shear stress at the interface increases continuously with time until the local shear stress reaches a critical *depinning* stress σ_c, after which a rapid local slip occurs, but with the rubber patch in continuous adhesive contact with the substrate. During the local slip the elastic deformation energy stored in the rubber during the loading phase will be dissipated partly inside the rubber (in a volume of order D^3) and partly at the interface. The deformation field in the vicinity of a stress domain of area $\sim D^2$ will extend a distance $\sim D$ into the rubber block; we denote this basic unit (volume $\sim D^3$) as a *stress block* (see volume elements surrounded by dashed lines in Fig. 2(a)).

Figure 2 illustrates three other mechanisms of rubber friction, which all depend on the rubber-substrate adhesional interaction. Figure 2(b) illustrates a case where a rubber block is sliding on a smooth wavy substrate. Here we assume only roughness (waviness) on a single length scale, *i.e.*, the substrate bumps have no roughness on length scales smaller than the lateral size of the bumps. In this case, if the adhesional interaction (and the external applied normal load) is unable to bring the rubber into perfect contact with the substrate, (as in the figure), during sliding opening and closing cracks will occur at the exit and the front of each asperity contact region. In general, negligible bulk viscoelastic energy dissipation occurs at the closing crack, while a huge energy dissipation may occur at the opening crack [12,13]. It has been shown that in some cases the dominant contribution to the friction force arises from the energy "dissipation" at the opening cracks [12,13].

If the substrate has small-amplitude roughness, the adhesive rubber-substrate interaction may (even in the absence of an external load) lead to complete contact between the rubber and the substrate at the sliding interface (see Fig. 2(c)). In this case, during sliding viscoelastic deformations will occur in the bulk of the rubber in the vicinity of the substrate, which will contribute to the observed friction. This contribution can be calculated using the theory developed in references [3,14].

Finally, for very soft rubber it has often been observed that detachment waves propagate throughout the entire contact area, from its advancing to the trailing edge, see Figure 2(d). Schallamach [15] first discovered these waves at "high" sliding velocities and for (elastically) soft rubber. Roberts and Thomas [12,16] have shown that when such instabilities occur, the frictional stress is mainly due to the energy dissipation at the opening crack, *i.e.*, similar to the situation in Figure 2(b).

In this paper we study the rubber friction process shown in Figure 2(a). This is probably the most important rubber friction mechanism in most applications involving *very* smooth surfaces. In Section 2 (and App. A) we consider the fluctuating shear stress inside a viscoelastic solid, which results from the thermal motion of the atoms or molecules in the solid. At the nanoscale, the thermal fluctuations are very strong giving stress fluctuations in the MPa-range, which is similar to the depinning stresses which typically occur at solid-rubber interfaces, illustrating the crucial importance of thermal fluctuations for rubber friction on smooth surfaces. In Section 3 (and Apps. B and C) we develop a detailed model which takes into account the influence of thermal fluctuations on the depinning of small contact areas (stress domains) at the rubber-substrate interface. The theory predicts that the velocity dependence of the macroscopic shear stress has a bell-shaped form (see Sect. 4), and that the low-velocity side exhibits the same temperature dependence as the bulk

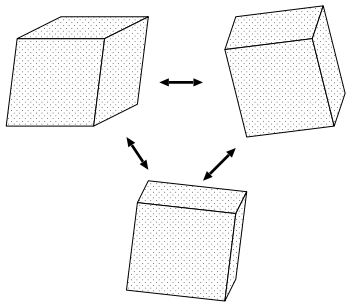

Fig. 3. The thermal motion of the atoms in a solid gives rise to shape fluctuations for a small volume element in the solid (schematic).

viscoelastic modulus, in qualitative agreement with experimental data (Sect. 5). In Section 5 we also discuss the role of the surface roughness, which exists even on very smooth surfaces. We show that the countersurfaces used in the study by Vorvolakos and Chaudhury [17] have such small surface roughness that the roughness contributes negligibly to the friction. Section 6 contains the summary and conclusion.

2 Brownian motion in viscoelastic solids

A small particle in a liquid performs random motion caused by the impact of the surrounding liquid molecules. Similarly, a small volume element in a viscoelastic solid performs *shape fluctuations* as a result of the thermal motion of the atoms or molecules in the solid, see Figure 3. Here we will estimate the magnitude of the fluctuating shear stress which acts on any (internal) surface in a viscoelastic solid.

Assume that $\mathbf{u}(\mathbf{x},t)$ is the displacement vector in an infinite viscoelastic solid. The equation of motion for $\mathbf{u}$ is

$$\rho\frac{\partial^2\mathbf{u}}{\partial t^2} = \hat{\mu}\nabla^2\mathbf{u} + \big(\hat{\mu}+\hat{\lambda}\big)\nabla\nabla\cdot\mathbf{u} + \mathbf{f}, \tag{1}$$

where $\hat{\mu}$ and $\hat{\lambda}$ are time integral operators, *e.g.*,

$$\hat{\mu}G(t) = \int_{-\infty}^{t} \mathrm{d}t'\,\mu(t-t')G(t'),$$

and where $\mathbf{f}(\mathbf{x},t)$ is a randomly fluctuating-force density. If we define the Fourier transform

$$f_i(\mathbf{k},\omega) = \frac{1}{(2\pi)^4}\int \mathrm{d}^3x\mathrm{d}t\, f_i(\mathbf{x},t)e^{-i(\mathbf{k}\cdot x-\omega t)}$$

and

$$f_i(\mathbf{x},t) = \int \mathrm{d}^3k\mathrm{d}\omega\, f_i(\mathbf{k},\omega)e^{i(\mathbf{k}\cdot x-\omega t)}$$

we can write

$$\langle f_i(\mathbf{k},\omega)f_j(\mathbf{k}',\omega')\rangle = -\frac{k_{\mathrm{B}}T}{\pi\omega}(2\pi)^{-3} \times\left(\mathrm{Im}\,\mu(\omega)k^2\delta_{ij} + \mathrm{Im}\,\frac{\mu(\omega)}{1-2\nu}k_ik_j\right) \times\delta(\mathbf{k}+\mathbf{k}')\delta(\omega+\omega'), \tag{2}$$

where $\nu=\lambda/2(\mu+\lambda)$ and where

$$\mu(\omega) = \int_0^\infty \mathrm{d}t\,\mu(t)e^{i\omega t}.$$

Let us study the fluctuating stress in the solid. The average stress $\langle\sigma_{ij}\rangle = 0$ but the average of the square of any components of σ_{ij} will be finite. Here we consider the magnitude of the fluctuating shear stress within some plane which we can take to be the xy plane. Thus we consider

$$\big\langle\sigma_\parallel^2\big\rangle = \big\langle\sigma_{zx}^2+\sigma_{zy}^2\big\rangle = 2\big\langle\sigma_{zx}^2\big\rangle.$$

In Appendix A we show that

$$\bar{\sigma}_\parallel^2 \equiv \big\langle\sigma_\parallel^2\big\rangle = k_{\mathrm{B}}TCD^{-3}(E_\infty - E_0), \tag{3}$$

where $E_0=E(0)$ and $E_\infty=E(\infty)$ are the low- and high-frequency rubber modulus (both real), respectively, and where

$$C = \frac{8\pi(4-5\nu)}{45(1-\nu^2)}\,. \tag{4}$$

In deriving (3) we have used the relation $\mu=E/2(1+\nu)$, where $E(\omega)$ is Young's (viscoelastic) modulus and ν the Poisson ration which is assumed to be independent of the frequency. In (3) D is a cut-off length, of order the distance between the cross-links, or larger. Assuming $\nu=0.5$ gives $C\approx 1.1$. In a typical case $E_\infty\approx 10^9\,\mathrm{Pa}\gg E_0$ and if $D=10\,\mathrm{nm}$ we get at room temperature $\bar{\sigma}_\parallel\approx 1\,\mathrm{MPa}$, which (typically) is of the same order of magnitude as the depinning stress at a rubber-substrate interface.

It is also interesting to estimate the fluctuation in the displacement $\mathbf{u}_\parallel$ and the fluctuation in the strain. Using the same approach as above one obtains (see App. A)

$$\big\langle u_\parallel^2\big\rangle = k_{\mathrm{B}}TC'D^{-1}\left(\frac{1}{E_0}-\frac{1}{E_\infty}\right),$$

where

$$C' = \frac{2(5-6\nu)(1+\nu)}{3(1-\nu)}\,.$$

In a similar way one can calculate the average of the square of the strain

$$\big\langle\epsilon_\parallel^2\big\rangle = \big\langle\epsilon_{zx}^2+\epsilon_{zy}^2\big\rangle = k_{\mathrm{B}}TC''D^{-3}\left(\frac{1}{E_0}-\frac{1}{E_\infty}\right),$$

where

$$C'' = \frac{32\pi(4-5\nu)(1+\nu)^2}{45(1-\nu^2)}\,.$$

With $E_0=1\,\mathrm{MPa}$ and $D=10\,\mathrm{nm}$ one gets at room temperature $\bar{u}_\parallel\approx 1\,\mathrm{nm}$ and $\bar{\epsilon}_\parallel\approx 0.3$.

The analysis above indicates that, on a length scale of $\sim 10\,\mathrm{nm}$, very large strain and stress fluctuations occur in normal rubber. The stress fluctuations are of similar magnitude as the (typical) rubber-substrate depinning stress, suggesting that thermally excited transitions over the (lateral) energy barriers play a crucial role in rubber friction on smooth substrates. However, the stress fluctuations ($\sim 1\,\mathrm{MPa}$) are negligible compared to the stress necessary for detaching a rubber patch in the normal direction, since the latter is determined by the adhesional

stress [18,19] which typically is of order 1 GPa. Thus, rubber sliding on smooth surfaces never involves (thermally activated) detachment of rubber from the substrate surface, but only (lateral) sliding of rubber patches (the lateral depinning stress is typically 100–1000 times smaller than the adhesional stress). (Detached areas may form and propagate at the interface (as for Schallamach waves, see fig. 2(d)), but in these cases they are generated by the external applied stress, and depend on the shape of the bodies; the detached regions usually form at the edge of the rubber-substrate contact region, where elastic instabilities (*e.g.*, "buckling") of the rubber may occur [20].) In the next section we will develop a model of rubber sliding friction based on the picture presented above.

3 Theory

We consider a rubber block with a smooth flat surface sliding on a perfectly smooth and flat substrate. We assume that the adhesive rubber-substrate interaction will result in perfect contact between the two solids (*i.e.*, we assume that no Schallamach waves occur at the interface). During sliding at low velocities, small (nanometer-sized) regions (stress blocks) at the sliding interface will perform stick-slip motion. We model the real physical system in Figure 4(a) with the block-spring model shown in Figure 4(b). However, the springs in the model are not elastic springs but *viscoelastic* springs determined by the viscoelastic modulus of the rubber (see below). Furthermore, the blocks in the model experience not only the stress from the substrate and the forces from the springs, but also randomly fluctuating (in time) forces derived from the thermal motion of the molecules in the solid. The strength of the fluctuating forces is determined by the temperature and by the viscoelastic properties of the springs via the fluctuation-dissipation theorem. The combination of the (thermal) fluctuating forces, and the forces derived from the external pulling of the upper surface of the rubber block, and the stress acting on the bottom surface of the block from the substrate, determine the motion of the stress blocks.

We assume that the motion at low sliding velocity occurs by a thermally activated process, where small surface areas or "patches" of rubber at the interface perform stick-slip motion. We will refer to these "patches" as stress domains. The stress domains are pinned by the substrate potential, and we assume that some characteristic shear stress σ_c must be reached before local slip can occur. Thus, the pinning force $F_c = \sigma_c D^2$, where D is the characteristic linear size of a stress domain.

The equation of motion for the coordinate q_i of the stress domain i is assumed to be

$$m\ddot{q}_i = \hat{k}_z(x - q_i) + \hat{k}_x(q_{i+1} - q_i) + \hat{k}_x(q_{i-1} - q_i) + f_i + F_i\,, \tag{5}$$

where $x = vt$ and where $\hat{k}_z$ is a time integral operator,

$$\hat{k}_z x(t) = \int_{-\infty}^{t} \mathrm{d}t'\; k_z(t - t')x(t'), \tag{6}$$

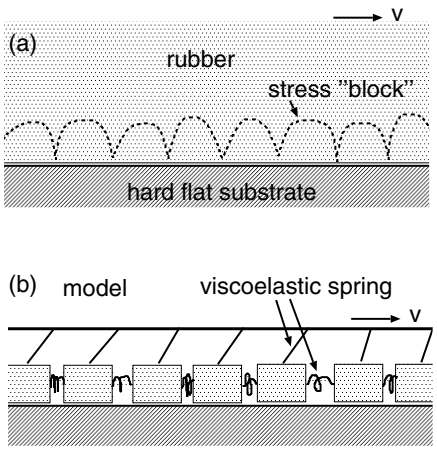

Fig. 4. (a) Rubber block in adhesive contact with a flat substrate. During sliding at low velocities, small rubber volume elements (stress blocks) perform stick-slip motion. (b) The model used in the mathematical description of the system in (a). The viscoelastic springs k are determined by the rubber viscoelastic modulus and by the lateral size D of the stress blocks via $k(\omega) \approx E(\omega)D$.

and similar for $\hat{k}_x$. We consider N stress domains, $i = 1, \ldots, N$, and assume periodic boundary conditions so that $q_0 = q_N$. In (5), $f_i(t)$ is a stochastically fluctuating force which results from the thermal motion of the rubber molecules. The force F_i acts on the stress domain i from the substrate and is defined as follows: When the stress domain i slips, then $F_i = -m\eta\dot{q}_i$. In the pinned state, F_i is just large enough to balance the total force exerted by the stress block on the substrate:

$$F_i = -\hat{k}_z(x - q_i) - \hat{k}_x(q_{i+1} - q_i) - \hat{k}_x(q_{i-1} - q_i) - f_i\,. \tag{7}$$

Slip will start when $|F_i|$ reaches a critical value F_c, either as a result of the external applied force or as a result of a large enough thermal fluctuation, or, in general, as a combination of both these effects.

We define the Fourier transform

$$x(\omega) = \frac{1}{2\pi}\int \mathrm{d}t\, x(t)e^{i\omega t}, \tag{8}$$

$$x(t) = \int \mathrm{d}\omega\, x(\omega)e^{-i\omega t}. \tag{9}$$

The fluctuating force $f_i(t)$ results from the thermal motion of the rubber molecules and must satisfy the fluctuation-dissipation theorem. That is, if we write

$$\hat{K}_{ij}q_j = \hat{k}_z q_i - \hat{k}_x(q_{i+1} - q_i) - \hat{k}_x(q_{i-1} - q_i), \tag{10}$$

then from the theory of Brownian motion (see App. D)

$$\langle f_i(\omega)f_j(\omega')\rangle = -\frac{k_B T}{\pi\omega}\,\mathrm{Im}\,K_{ij}(\omega)\delta(\omega + \omega'), \tag{11}$$

where

$$K_{ij}(\omega) = \int_0^\infty \mathrm{d}t\, K_{ij}(t)e^{i\omega t}$$

and (for $t > 0$)

$$K_{ij}(t) = \frac{1}{2\pi}\int \mathrm{d}\omega\, K_{ij}(\omega)e^{-i\omega t}.$$

If we write the elastic modulus as [21]

$$E(\omega) = E_\infty\left(1 - \sum_n \frac{h_n}{1 - i\omega\tau_n}\right), \tag{12}$$

we get

$$K_{ij}(\omega) = K_{ij}^\infty - K_{ij}^\infty \sum_n \frac{h_n}{1 - i\omega\tau_n}, \tag{13}$$

where

$$K_{ij}^\infty = \left(k_z^\infty + 2k_x^\infty\right)\delta_{ij} - k_x^\infty\left(\delta_{i,j+1} + \delta_{i,j-1}\right).$$

Equation (12) gives

$$\mathrm{Im}\, K_{ij}(\omega) = -K_{ij}^\infty \sum_n \frac{h_n\tau_n\omega}{|1 - i\omega\tau_n|^2}. \tag{14}$$

Substituting (13) in (11) gives

$$\langle f_i(\omega)f_j(\omega')\rangle = \frac{k_\mathrm{B}T}{\pi}K_{ij}^\infty \sum_n \frac{h_n\tau_n}{|1 - i\omega\tau_n|^2}\delta(\omega + \omega'). \tag{15}$$

In Appendices B and C we show how the equations above can be reformulated in a form convenient for numerical calculations.

In the calculations presented below we have assumed that a sliding block returns to the pinned state when the shear stress $|\sigma| < \sigma_{c1} = \lambda\sigma_c$, where $\sigma_c = F_c/D^2$ is the depinning stress and $\lambda < 1$. We assume that when the shear stress has decreased below σ_{c1} the block returns to the pinned state with the probability rate w, and we use random number to determine when the transition actually takes place. Thus, if r is a random number uniformly distributed in the interval $[0, 1]$, then if $|\sigma| < \sigma_{c1}$ we assume that the stress block returns to the pinned state during the time interval δt (the time integration step length) if $w\delta t > r$. In the simulations below we use $w \leq 10^{12}\,\mathrm{s}^{-1}$ and $\lambda = 0.1$. We use $\delta \approx 10^{-13}\,\mathrm{s}$ in most of our simulations so that the condition $w\delta t \ll 1$ is satisfied, and the results presented below do not depend on the time step δt.

The linear size of the stress blocks, D, is most likely determined by the elastic modulus and the depinning shear stress σ_c as follows. The stress block is the smallest unit which is able to slide as a coherent unit and can be determined as follows. The depinning force is $F_c = \sigma_c D^2$. If the stress σ acts at the bottom surface of a stress block, it will move a distance x determined by $kx = \sigma D^2$, where $k \approx ED$, where E is the elastic modulus. The stress block experiences a quasi-periodic pinning potential from the substrate, characterized by a lattice constant a of order a few ångströms. Thus, the stress block will in general be able to occupy a "good" binding position in the corrugated substrate potential only if ka is less than the pinning potential [22]. The condition $ka = F_c$ gives the size D of the pinned domains. Using $F_c = \sigma_c D^2$ and $k \approx ED$ gives

$$D \approx Ea/\sigma_c.$$

In a typical case $E \approx (E_0E_\infty)^{1/2} \approx 100\,\mathrm{MPa}$, $\sigma_c \approx 1\,\mathrm{MPa}$ and a a few ångströms, giving $D = 30\,\mathrm{nm}$. Since D increases when the elastic modulus increases, the present theory indicates that the friction should increase with increasing elastic modulus. This is exactly what has been observed in friction studies for smooth surfaces [17]. Since the elastic modulus E depends on frequency, during sliding the size D of the stress domains may depend on the sliding velocity, but we have not taken this effect into account in this paper.

4 Numerical results

We now present numerical results for styrene butadiene rubber both with and without filler using the measured [23] viscoelastic modulus $E(\omega)$. In reference [21] we have shown how the parameters h_n and τ_n in the representation (12) of $E(\omega)$ can be determined directly from

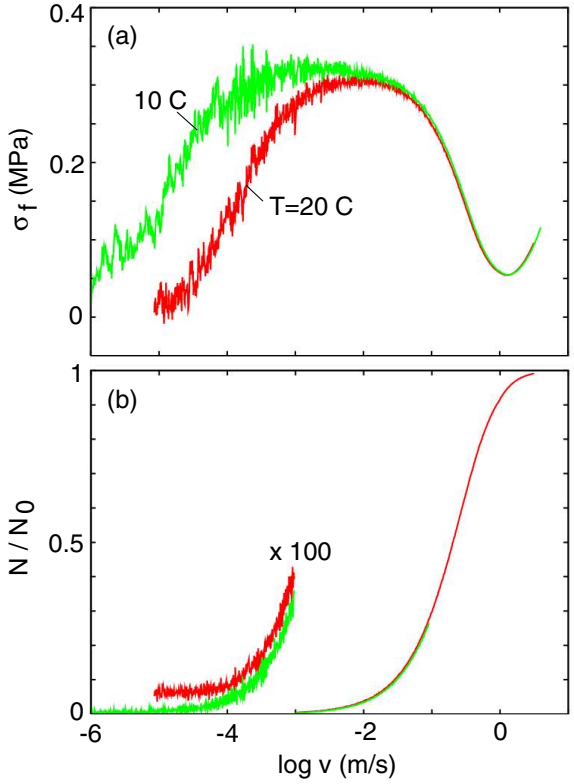

Fig. 5. (a) The frictional shear stress σ_f and (b) the fraction of slipping surface area N/N_0 as a function of the logarithm (with 10 as basis) of the sliding velocity of the rubber block. For styrene butadiene copolymer with 60% carbon black and for two different temperatures, $T = 10\,^\circ\mathrm{C}$ and $20\,^\circ\mathrm{C}$. In the calculation we have used the (zero-temperature) depinning stress $\sigma_c = 1\,\mathrm{MPa}$ and the stress block size $D = 30\,\mathrm{nm}$. The number of stress blocks was 128. The viscous friction coefficient during steady sliding $\eta = 0.03$ (natural units) and the critical stress below which steady sliding becomes metastable $\sigma_{c1} = 0.1\sigma_c = 0.1\,\mathrm{MPa}$. The probability rate per unit time to return to the pinned state when $\sigma < \sigma_{c1}$ is $w = 2 \times 10^{10}\,\mathrm{s}^{-1}$.

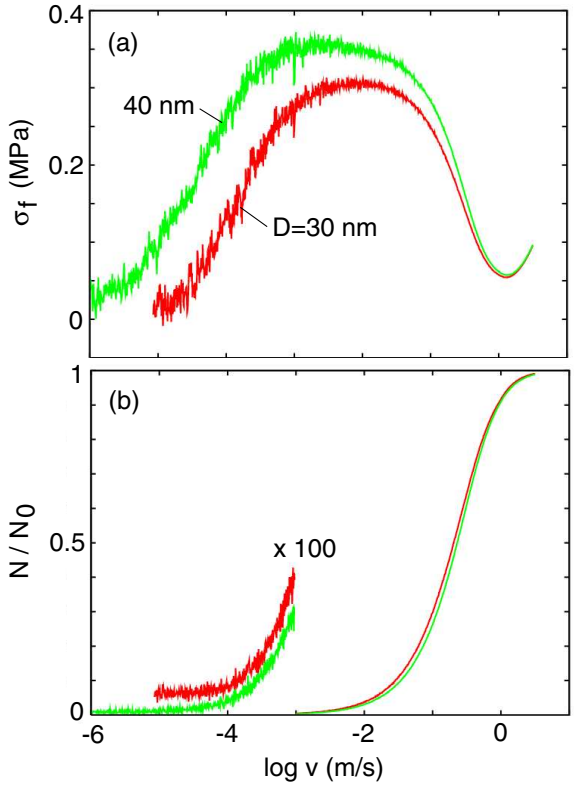

Fig. 6. The frictional shear stress σ_f as a function of the logarithm of the sliding velocity of the rubber block. For the temperature $T = 20\,^\circ$C and for the stress block sizes $D = 30$ and 40 nm. All other parameters as in Figure 5.

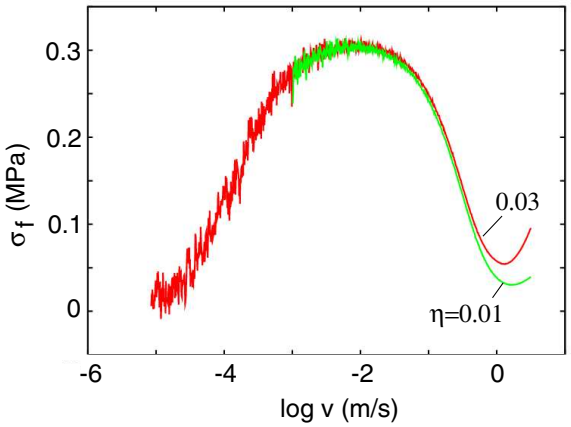

Fig. 7. The frictional shear stress σ_f as a function of the logarithm of the sliding velocity of the rubber block. For the temperature $T = 20\,^\circ$C and for the viscous friction coefficients $\eta = 0.03$ and 0.01 (natural units). All other parameters as in Figure 5.

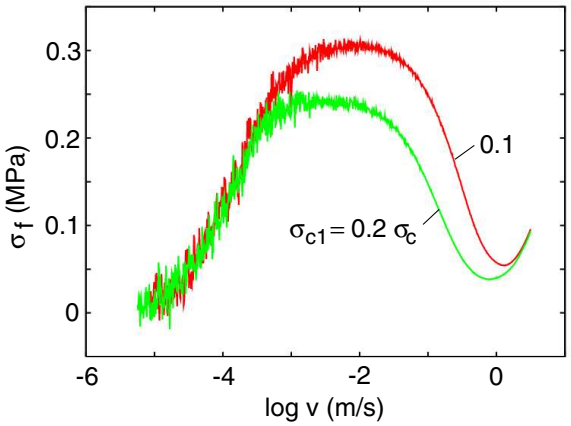

Fig. 8. The frictional shear stress σ_f as a function of the logarithm of the sliding velocity of the rubber block. For the temperature $T = 20\,^\circ$C and for the critical stresses (below which steady sliding becomes metastable) $\sigma_{c1} = 0.1\sigma_c = 0.1$ MPa and 0.2 MPa. All other parameters as in Figure 5.

the measured $E(\omega)$. The (τ_n, h_n) data used in the present study is shown in Figure B2 in reference [21].

Figure 5(a) shows the frictional shear stress σ_f and Figure 5(b) the fraction of slipping surface area N/N_0 as a function of the logarithm (with 10 as basis) of the sliding velocity of the rubber block. The results are for styrene butadiene copolymer with 60% carbon black, and for two different temperatures, $T = 10\,^\circ$C and $20\,^\circ$C. Note that the low-velocity part ($v < v_1$, where $v_1 \approx 10^{-2}$ m/s is the velocity at which the friction is maximal) of the friction curve is shifted by ~ 1 decade towards lower velocities when the temperature is reduced from 20 to $10\,^\circ$C. This is identical to the change in the (bulk) viscoelastic shift factor a_T, which changes by a factor of ~ 10 during the same temperature change. Figure 5(b) shows that the number of moving stress blocks is basically temperature independent for sliding velocities $v > v_1 \approx 10^{-2}$ m/s, *i.e.*, for $v > v_1$ the fluctuating force arising from the finite temperature has a negligible influence on the friction force. For $v < v_1$ more stress blocks are depinned at a higher temperature because the fluctuating force is larger at a higher temperature. Note also that the maximal shear stress $\sigma_f \approx 0.3$ MPa is about 30% of the depinning stress $\sigma_c = 1$ MPa.

Figure 6(a) shows the frictional shear stress σ_f and Figure 6(b) the fraction of sliding blocks, as a function of the logarithm of the sliding velocity. In the calculation we have used $T = 20\,^\circ$C and the stress block sizes $D = 30$ and 40 nm. When the stress block size increases, the pinning force $\sigma_c D^2$ increases, and it is necessary to go to lower sliding velocities in order for temperature effects to manifest themselves (as a decrease in the frictional shear stress).

Figure 7 shows the frictional shear stress σ_f as a function of the logarithm of the sliding velocity. Results are shown for two different viscous friction coefficients $\eta = 0.03$ and 0.01 (natural units). As expected, η is only important at relative high sliding velocities.

Figure 8 shows how σ_f depends on the sliding velocity for two different values (0.1 and 0.2 MPa) of the critical stress σ_{c1} below which the sliding patch can return to the pinned state.

Figure 9 shows the frictional shear stress σ_f as a function of the logarithm of the sliding velocity of the rubber block for two different values (2×10^{10} and 10^{12} s^{-1}) of the probability rate per unit time to return to the pinned

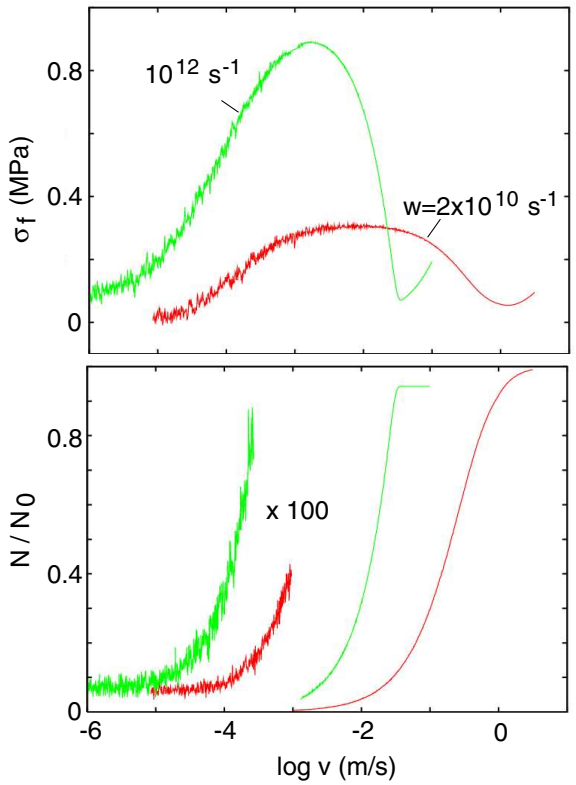

Fig. 9. The frictional shear stress σ_f as a function of the logarithm of the sliding velocity of the rubber block. For the temperature $T = 20\,^\circ$C and for the probability rates per unit time to return to the pinned state (when $\sigma < \sigma_{c1}$) $w = 2 \times 10^{10}\,\mathrm{s}^{-1}$ and $w = 10^{12}\,\mathrm{s}^{-1}$. All other parameters as in Figure 5.

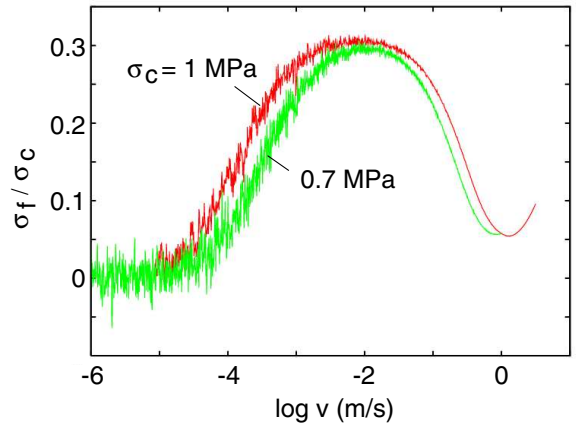

Fig. 10. The frictional shear stress σ_f as a function of the logarithm of the sliding velocity of the rubber block. For the temperature $T = 20\,^\circ$C and for the (zero-temperature) depinning stresses $\sigma_c = 1\,$MPa and $\sigma_c = 0.7\,$MPa. All other parameters as in Figure 5.

state when $\sigma < \sigma_{c1}$. Figure 10 shows similar results for two different values (1 and 0.7 MPa) of the depinning stress σ_c.

Figure 11 shows the frictional shear stress σ_f as a function of the logarithm of the sliding velocity of the rubber block for an unfilled styrene butadiene (SB) copolymer for two different values (30 and 40 nm) of the size D of a pinned region.

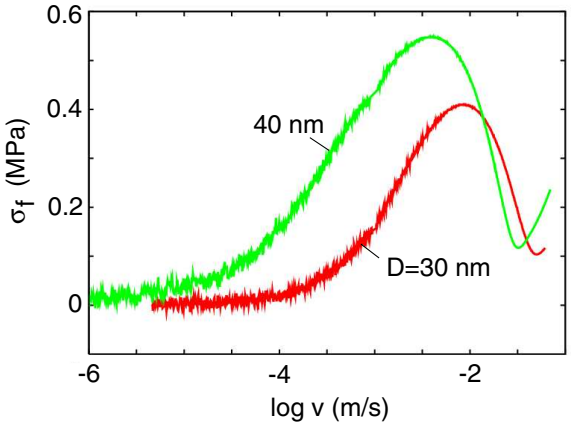

Fig. 11. The frictional shear stress σ_f as a function of the logarithm of the sliding velocity of the rubber block. For unfilled styrene butadiene (SB) copolymer for $T = 20\,^\circ$C. In the calculation we have used the (zero-temperature) depinning stress $\sigma_c = 1\,$MPa and the stress block size $D = 30\,$nm and 40 nm. The number of stress blocks was 128. The viscous friction coefficient during steady sliding $\eta = 0.03$ (natural units), and the critical stress below which steady sliding becomes metastable $\sigma_{c1} = 0.1\sigma_c = 0.1\,$MPa. The probability rate per unit time to return to the pinned state when $\sigma < \sigma_{c1}$ is $w = 10^{12}\,\mathrm{s}^{-1}$.

5 Discussion

Vorvolakos and Chaudhury [17] have performed a very detailed experimental study of sliding friction for silicon rubber on hard flat (passivated) substrates (see also Refs. [24–28] for other studies of elastomer friction). They used silicon rubbers with many different (low-frequency) elastic moduli E.

In Figure 12 we show the velocity dependence of the shear stress as measured at different temperatures $T =$ 298 (open circles), 318 (gray circles) and 348 K (black circles) for a silicon rubber with the low-frequency elastic modulus $E \approx 5\,$MPa. The experimental data on the low-velocity side can be shifted to a single curve when plotted as a function of va_T, see reference [17]. This is in accordance with our model calculations (see Sect. 4) and shows the direct involvement of the rubber bulk in the sliding dynamics.

Vorvolakos and Chaudhury [17] have shown that the frictional shear stress for all the studied rubbers increases with increasing elastic modulus. This is in qualitative agreement with our theory since, as explained in Section 3, as E increases we expect the linear size D of the stress domains to increase, which will increase the sliding friction (see Figs. 6 and 11).

In the experiments by Grosch [24] it was observed that the friction on smooth surfaces has a bell-like shape with a maximum at some characteristic velocity $v = v_1$. We observe the same general behavior, but with some important differences. Thus, the experimental data of Grosch was observed to obey the WLF transform. That is, the full friction curve could be constructed by performing measurements in a very limited velocity range and at different temperatures, and then use the WLF transform to shift

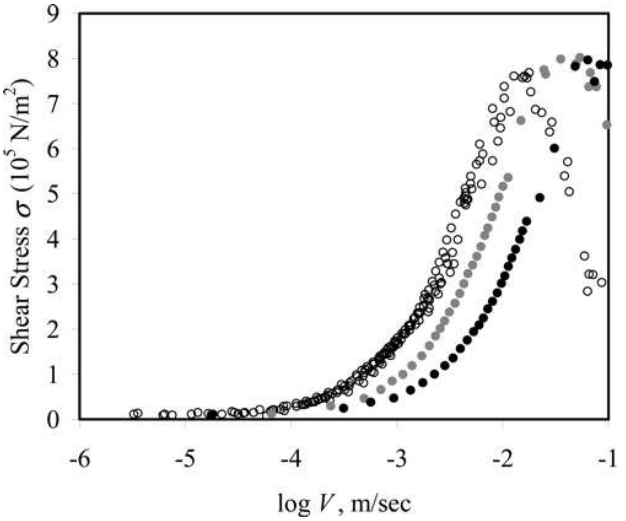

Fig. 12. Shear stress as a function of velocity and temperature for a silicon elastomer (low-frequency elastic modulus $E \approx 5\,\mathrm{MPa}$) sliding on a Si wafer covered by an inert self-assembled–monolayers film. Open circles, gray circles and black circles represent data at 298, 318 and 348 K, respectively. Adapted from reference [17].

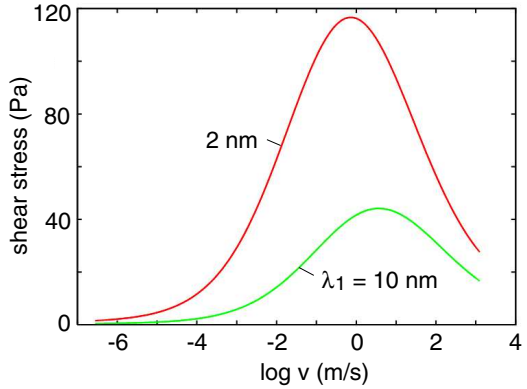

Fig. 13. The frictional shear stress σ_f as a function of the logarithm of the sliding velocity of the rubber block. For styrene butadiene copolymer with 60% carbon black and for $T = 40\,^\circ\mathrm{C}$. The friction is entirely due to the surface roughness of the substrate which is assumed to be self-affine fractal with the fractal dimension $D_f = 2.3$ and the root-mean-square roughness 0.5 nm. The long-wavelength and short-wavelength roll-off wave vectors $q_0 = 2\pi/\lambda_0$ and $q_1 = 2\pi/\lambda_1$, where $\lambda_0 = 100\,\mu\mathrm{m}$ and $\lambda_1 = 2\,\mathrm{nm}$ (upper curve) and 10 nm (lower curve).

the measured data to a single temperature. We also find that our calculated friction obeys the WLF transform for $v < v_1$, but not for $v > v_1$. Thus, the decrease in the friction which we observe for $v > v_1$ is nearly temperature independent. The difference between our prediction and the Grosch results can be understood as follows: Most likely, the decrease of the friction for $v > v_1$ in the Grosch experiment is related to a decrease in the area of real contact with increasing sliding velocity. The Grosch experiments where performed on smooth but wavy glass, and the area of real contact depends on the effective elastic modulus of the rubber. Thus, as the sliding velocity increases or, equivalently, the temperature decreases, the rubber becomes stiffer and the area of real contact decreases. Hence, if the shear stress remains constant at high sliding velocity (as we indeed observe in our calculations if the calculations are performed at *low velocities* and different temperatures, and shifted to higher velocity using the WLF equation), then the friction force will decrease with increasing sliding velocity because of the decrease in the area of real contact.

The experiments by Vorvolakos and Chaudhury [17] was performed on (passivated) silicon wafers with the root-mean-square roughness of at most 0.5 nm. For such smooth surfaces the adhesive rubber-substrate interaction will, even in the absence of a squeezing pressure, give rise to complete contact between the rubber and the substrate within the nominal contact area. For this case we have applied the rubber friction theory developed in reference [3] to obtain the contribution to the frictional shear stress from the roughness-induced bulk viscoelastic deformations in the rubber (Fig. 2(c)). We have assumed that the substrate is self-affine fractal with the fractal dimension $D_f = 2.3$ and the long-distance roll-off wavelength $\lambda_0 = 100\,\mu\mathrm{m}$. We have included roughness components down to the short-distance (cut-off) wavelength λ_1. In Figure 13 we show the resulting frictional shear stress (assuming perfect contact at the sliding interface) using $\lambda_1 = 10\,\mathrm{nm}$ and 2 nm. The smallest possible λ_1 is determined by an atomic distance but a more likely cut-off length in the present case is the mean distance between rubber cross-links, which is of order a few nanometers. The calculated maximal shear stress is of order $\sim 100\,\mathrm{Pa}$, which is a factor $\sim 10^4$ smaller than the shear stress observed in reference [17]. Hence we conclude that the surface roughness in the measurements of Vorvolakos and Chaudhury has a negligible influence on the observed frictional shear stress. However, the surfaces used in reference [17] are exceptionally smooth, and surface roughness can be very important for rubber friction for surfaces of more common use in rubber applications, *e.g.*, for rubber sealing.

6 Summary and conclusion

We have studied the sliding friction for viscoelastic solids, *e.g.*, rubber, on hard flat substrate surfaces. We have shown that the fluctuating shear stress, which result from the thermal motion of the atoms or molecules in a viscoelastic solid, gives rise to very strong stress fluctuations, which at the nanoscale are in the MPa-range. This is similar to the depinning stresses which typically occur at solid-rubber interfaces, indicating the crucial importance of thermal fluctuations for rubber friction on smooth surfaces. We have developed a detailed model which takes into account the influence of thermal fluctuations on the depinning of small contact patches (stress domains) at the rubber-substrate interface. The theory predicts that the velocity dependence of the macroscopic shear stress has a bell-shaped form, and that the low-velocity side exhibits a similar temperature dependence as the bulk

viscoelastic modulus, in qualitative agreement with experimental data. Finally, we have discussed the influence of small-amplitude substrate roughness on rubber sliding friction and shown that it gives a negligible contribution to the friction in the experiments of Vorvolakos and Chaudhury [17].

A.I.V. and B.N.J.P. thank DFG for support, and the EU for support within the "Natribo" network of the European Science Foundation.

Appendix A. Stress and strain fluctuations in viscoelastic solids

Let us study the fluctuating stress in the solid. The average stress $\langle\sigma_{ij}\rangle = 0$ but the average of the square of any components of σ_{ij} will be finite. Here we consider the magnitude of the fluctuating shear stress within some plane which we can take to be the xy plane. Thus, we consider

$$\langle\sigma_\parallel^2\rangle = \langle\sigma_{zx}^2 + \sigma_{zy}^2\rangle = 2\langle\sigma_{zx}^2\rangle.$$

The stress tensor

$$\sigma_{ij} = \hat{\mu}(u_{i,j} + u_{j,i}) + \hat{\lambda}u_{k,k}\delta_{ij}.$$

Thus we get

$$\sigma_{zx} = \hat{\mu}(u_{z,x} + u_{x,z})$$

and

$$\begin{aligned}\langle\sigma_\parallel^2\rangle = {} & 4\langle(\hat{\mu}u_{z,x})^2 + \hat{\mu}u_{z,x}\hat{\mu}u_{x,z}\rangle = \\ & -4\int \mathrm{d}^3k\mathrm{d}^3k'\mathrm{d}\omega\mathrm{d}\omega'\mu(\omega)\mu(\omega') \\ & \times(k_xk_x'\langle u_z(\mathbf{k},\omega)u_z(\mathbf{k}',\omega')\rangle \\ & +k_xk_z'\langle u_z(\mathbf{k},\omega)u_x(\mathbf{k}',\omega')\rangle). \end{aligned} \quad (A.1)$$

Using (1) and neglecting inertia effects gives

$$\begin{aligned}\mathbf{u}(\mathbf{k},\omega) = {} & \frac{1}{\mu(\omega)k^2 + (\mu(\omega)+\lambda(\omega))\mathbf{kk}}\cdot\mathbf{f}(\mathbf{k},\omega) = \\ & \frac{1}{\mu(\omega)k^2}\left(1 - \frac{1}{2(1-\nu)}\frac{\mathbf{kk}}{k^2}\right)\cdot\mathbf{f}(\mathbf{k},\omega). \end{aligned} \quad (A.2)$$

Using (A.2) and (2) and assuming that ν is frequency independent gives

$$\langle\sigma_\parallel^2\rangle = -k_\mathrm{B}TC3(2\pi)^{-5}\int \mathrm{d}^3k\mathrm{d}\omega\,\frac{1}{\omega}\,\mathrm{Im}\,E(\omega), \quad (A.3)$$

where

$$C = \frac{8\pi(4-5\nu)}{45(1-\nu^2)}.$$

In deriving (A.3) we have used the relation $\mu = E/2(1+\nu)$, where $E(\omega)$ is Young's (viscoelastic) modulus. The shear stress when we only include wave vectors up to $k = 2\pi/D$ (where D is a cut-off length, of order the distance between the cross-links, or larger) is given by

$$\langle\sigma_\parallel^2\rangle = -k_\mathrm{B}TCD^{-3}\frac{2}{\pi}\int_0^\infty \mathrm{d}\omega\,\frac{1}{\omega}\,\mathrm{Im}\,E(\omega).$$

Using the *sum rule* [12,13]

$$\frac{2}{\pi}\int_0^\infty \mathrm{d}\omega\,\frac{1}{\omega}\,\mathrm{Im}\,E(\omega) = E_0 - E_\infty,$$

where $E_0 = E(0)$ and $E_\infty = E(\infty)$ are the low- and high-frequency rubber modulus (both real), respectively, we get

$$\bar{\sigma}_\parallel^2 \equiv \langle\sigma_\parallel^2\rangle = k_\mathrm{B}TCD^{-3}(E_\infty - E_0).$$

Assuming $\nu = 0.5$ gives $C \approx 1.1$.

It is also interesting to estimate the fluctuation in the displacement $\mathbf{u}_\parallel$ and the fluctuation in the strain. Using the same approach as above one obtains

$$\langle u_\parallel^2\rangle = \langle u_x^2 + u_y^2\rangle = k_\mathrm{B}TC'D^{-1}\frac{2}{\pi}\int_0^\infty \mathrm{d}\omega\,\frac{1}{\omega}\,\mathrm{Im}\left(\frac{1}{E(\omega)}\right),$$

where

$$C' = \frac{2(5-6\nu)(1+\nu)}{3(1-\nu)}.$$

If we use the sum rule [12,13]

$$\frac{2}{\pi}\int_0^\infty \mathrm{d}\omega\,\frac{1}{\omega}\,\mathrm{Im}\left(\frac{1}{E(\omega)}\right) = \frac{1}{E_0} - \frac{1}{E_\infty},$$

we get

$$\langle u_\parallel^2\rangle = k_\mathrm{B}TC'D^{-1}\left(\frac{1}{E_0} - \frac{1}{E_\infty}\right).$$

In a similar way one can calculate the average of the square of the strain

$$\langle\epsilon_\parallel^2\rangle = \langle\epsilon_{zx}^2 + \epsilon_{zy}^2\rangle = k_\mathrm{B}TC''D^{-3}\left(\frac{1}{E_0} - \frac{1}{E_\infty}\right),$$

where

$$C'' = \frac{32\pi(4-5\nu)(1+\nu)^2}{45(1-\nu^2)}.$$

Appendix B. Reformulation of the basic equations of motion

Using (13) we can write

$$\begin{aligned} & -K_{ij}(\omega)q_j(\omega) + k_z(\omega)x(\omega) = \\ & -K_{ij}^\infty q_j(\omega) + k_z^\infty x(\omega) - \sum_n h_n u_{ni}(\omega), \end{aligned} \quad (B.1)$$

where

$$u_{ni}(\omega) = \frac{-1}{1-i\omega\tau_n}K_{ij}^\infty q_j(\omega) + \frac{1}{1-i\omega\tau_n}k_z^\infty x(\omega) \quad (B.2)$$

or

$$u_{ni}(t) + \tau_n \dot{u}_{ni}(t) = -K^\infty_{ij} q_j(t) + k^\infty_z x + g_{ni}(t). \quad \text{(B.3)}$$

Here we have added a stochastically fluctuating force on the right-hand side of (B.3) which we can choose so as to reproduce the fluctuating force $f_i(t)$ in (5). That is, if we choose $g_{ni}(t)$ appropriately, we can remove the force $f_i(t)$ in (5). To this end we must choose

$$f_i(\omega) = -\sum_n \frac{h_n g_{nj}(\omega)}{1 - i\omega\tau_n} \quad \text{(B.4)}$$

with

$$g_{nj}(\omega) = N^{-1/2}\,\mathrm{Re}\sum_k M_{kn} e^{ikx_j}\xi_{kn}\,, \quad \text{(B.5)}$$

where

$$M_{kn} = \left(\frac{k_\mathrm{B}T\tau_n K^\infty_k}{\pi h_n}\right)^{1/2} \quad \text{(B.6)}$$

with the k-sum over

$$k = \frac{2\pi}{D}\frac{r}{N}, \qquad r = 0, 1, 2, \ldots, N-1.$$

Note that

$$K^\infty_k = k^\infty_z + k^\infty_x 2[1 - \cos(kD)] \quad \text{(B.7)}$$

is the (discrete) Fourier transform of K^∞_{ij}. In (B.5), ξ_{kn} are complex Gaussian random variables:

$$\xi_{kn} = \zeta_{kn} + i\eta_{kn}, \quad \text{(B.8)}$$

where

$$\langle \zeta_{kn}(\omega)\zeta_{k'n'}(\omega')\rangle = \delta_{nn'}\delta_{kk'}\delta(\omega+\omega'), \quad \text{(B.9)}$$

$$\langle \eta_{kn}(\omega)\eta_{k'n'}(\omega')\rangle = \delta_{nn'}\delta_{kk'}\delta(\omega+\omega'), \quad \text{(B.10)}$$

$$\langle \zeta_{kn}(\omega)\eta_{k'n'}(\omega')\rangle = 0. \quad \text{(B.11)}$$

Using (B.5) and (B.8) gives

$$g_{nj}(\omega) = N^{-1/2}\sum_k M_{kn}\left[\zeta_{kn}\cos(kx_j) - \eta_{kn}\sin(kx_j)\right]. \quad \text{(B.12)}$$

Using (B.9–B.11) gives

$$\begin{aligned}
&\langle g_{nl}(\omega) g_{n'l'}(\omega')\rangle = \\
&N^{-1}\sum_k M^2_{kn}\cos[k(x_l - x_{l'})]\delta_{nn'}\delta(\omega+\omega') = \\
&N^{-1}\sum_k M^2_{kn} e^{ik(x_l - x_{l'})}\delta_{nn'}\delta(\omega+\omega') = \\
&\frac{k_\mathrm{B}T\tau_n}{\pi h_n N}\sum_k K^\infty_k e^{ik(x_l - x_{l'})}\delta_{nn'}\delta(\omega+\omega') = \\
&\frac{k_\mathrm{B}T\tau_n}{\pi h_n} K^\infty_{ll'}\delta_{nn'}\delta(\omega+\omega'). \quad \text{(B.13)}
\end{aligned}$$

Using (B.4) and (B.13) gives

$$\langle f_i(\omega) f_j(\omega')\rangle = \frac{k_\mathrm{B}T}{\pi} K^\infty_{ij}\sum_n \frac{h_n\tau_n}{|1 - i\omega\tau_n|^2}\delta(\omega+\omega') \quad \text{(B.14)}$$

which agrees with (15).

Let us summarize the basic equations

$$\begin{aligned}
m\ddot{q}_i = {} & k^\infty_z(x - q_i) + k^\infty_x(q_{i+1} + q_{i-1} - 2q_i) \\
& - \sum_n h_n u_{ni} + F_i, \quad \text{(B.15)}
\end{aligned}$$

where

$$\begin{aligned}
u_{ni}(t) + \tau_n\dot{u}_{ni}(t) = {} & k^\infty_z(x - q_i) \\
& + k^\infty_x(q_{i+1} + q_{i-1} - 2q_i) + g_{ni}(t). \quad \text{(B.16)}
\end{aligned}$$

The random force

$$g_{nj}(\omega) = N^{-1/2}\,\mathrm{Re}\sum_k M_{kn} e^{ikx_j}\xi_{kn}(\omega), \quad \text{(B.17)}$$

where

$$M_{kn} = \left(\frac{k_\mathrm{B}T\tau_n K^\infty_k}{\pi h_n}\right)^{1/2}. \quad \text{(B.18)}$$

Appendix C. Numerical implementation

If D is the lateral size of a stress block, then the mass of a stress block $m = \rho D^3$. We introduce the spring constants $k^\infty_z = \alpha_z k^*$ and $k^\infty_x = \alpha_x k^*$, where $k^* = DE_\infty$, and where α_x and α_z are of order unity. We measure time in units of $\tau = (m/k^*)^{1/2}$ and distance in units of $l = F_\mathrm{c}/k^*$, where $F_\mathrm{c} = \sigma_\mathrm{c}D^2$ is the stress block pinning force. We also measure u in units of F_c and x in units of l. In these units (B.15) gives

$$\begin{aligned}
\ddot{q}_i = {} & \alpha^\infty_z(x - q_i) + \alpha^\infty_x(q_{i+1} + q_{i-1} - 2q_i) \\
& - \sum_n h_n u_{ni} + F_i/F_\mathrm{c}, \quad \text{(C.1)}
\end{aligned}$$

where (from (B.16))

$$\begin{aligned}
u_{ni}(t) + (\tau_n/\tau)\dot{u}_{ni}(t) = {} & \alpha_z(x - q_i) \\
& + \alpha_x(q_{i+1} + q_{i-1} - 2q_i) + g_{ni}(t). \quad \text{(C.2)}
\end{aligned}$$

The random force

$$g_{nj}(\omega) = N^{-1/2}\,\mathrm{Re}\sum_k M^*_{kn} e^{ikx_j}\xi_{kn}(\omega),$$

where

$$M^*_{kn} = M_{kn}/F_c = \left(\frac{k_\mathrm{B}T\tau_n K^\infty_k}{2\pi\Delta E k^* h_n}\right)^{1/2},$$

where $\Delta E = k^* l^2/2$. Note also that

$$\langle \zeta_{kn}(\omega)\zeta_{k'n'}(\omega')\rangle = \delta_{nn'}\delta_{kk'}\delta(\omega+\omega')$$

gives

$$\langle \zeta_{kn}(t)\zeta_{k'n'}(t')\rangle = 2\pi\delta_{nn'}\delta_{kk'}\delta(t-t').$$

In order to numerically integrate equations (C.1) and (C.2) we discretize time with the step length δt.

The (fluctuating) force δg_{ni} to be used for each time step in (C.2) can be written as

$$\delta g_{nj} = N^{-1/2}\,\mathrm{Re}\sum_k M^*_{kn} e^{ikx_j}\int_t^{t+\delta t}\mathrm{d}t'\xi_{kn}(t').$$

But if

$$\langle\zeta(t)\zeta(t')\rangle = 2\pi\delta(t-t')$$

we get

$$\langle(\delta\zeta)^2\rangle = \int_t^{t+\delta t}\mathrm{d}t'\mathrm{d}t''\langle\zeta(t')\zeta(t'')\rangle = 2\pi\delta t.$$

Thus we can write $\delta\zeta = (2\pi\delta t)^{1/2}G$, where G is a Gaussian random number with $\langle G^2\rangle = 1$. Thus, we take

$$\delta g_{nj} = N^{-1/2}\,\mathrm{Re}\sum_k M^*_{kn} e^{ikx_j}(2\pi\delta t)^{1/2}\big(G^{(1)}_{kn} + iG^{(2)}_{kn}\big),$$

where $G^{(1)}_{kn}$ and $G^{(2)}_{kn}$ are Gaussian random numbers. We can also write

$$\delta g_{nj} = N^{-1/2}\,\mathrm{Re}\sum_k \bar{M}_{kn} e^{ikx_j}\big(G^{(1)}_{kn} + iG^{(2)}_{kn}\big), \qquad \text{(C.3)}$$

where

$$\bar{M}_{kn} = \left(\frac{k_\mathrm{B}T}{\Delta E}\frac{\tau_n\delta t}{\tau^2}\frac{K^\infty_k}{h_n k^*}\right)^{1/2}.$$

The calculation of δg_{nj} (Eq. (C.3)) is conveniently performed using the fast-Fourier-transform method.

Appendix D. Memory friction and fluctuating force

Equation (11) is a standard result in the general theory of Brownian motion which can be derived in various ways. The most general proof is based on the memory function formalism as described, *e.g.*, in the book by D. Forster [29]. A simpler (but less general) derivation of equation (11) involves the study of a particle (coordinate $q(t)$) coupled to an infinite set of harmonic oscillators (the heat bath) (coordinates x_μ). For the readers' convenience, we briefly review this derivation here. The particle and the heat bath coordinates satisfy the equations of motion

$$m\ddot{q} + \sum_\mu \alpha_\mu x_\mu = 0, \qquad \text{(D.1)}$$

$$m_\mu\ddot{x}_\mu + m_\mu\omega^2_\mu x_\mu + \alpha_\mu q + m_\mu\eta_\mu\dot{x}_\mu = f_\mu\,, \qquad \text{(D.2)}$$

where

$$\langle f_\mu(t)f_\nu(t')\rangle = 2m_\mu\eta_\mu k_\mathrm{B}T\delta(t-t')\delta_{\mu\nu}. \qquad \text{(D.3)}$$

If we define

$$x_\mu(t) = \int \mathrm{d}\omega\, x_\mu(\omega)e^{-i\omega t},$$

$$x_\mu(\omega) = \frac{1}{2\pi}\int \mathrm{d}t\, x_\mu(t)e^{i\omega t}$$

and similar for q and f_μ, we get from (D.2)

$$x_\mu(\omega) = \frac{f_\mu(\omega) - \alpha_\mu q(\omega)}{m_\mu\big(\omega^2_\mu - \omega^2 - i\omega\eta_\mu\big)} \qquad \text{(D.4)}$$

and from (D.3),

$$\langle f_\mu(\omega)f_\nu(\omega')\rangle = m_\mu\eta_\mu k_\mathrm{B}T\delta(\omega+\omega')\delta_{\mu\nu}/\pi. \qquad \text{(D.5)}$$

From (D.4) we get

$$\sum_\mu \alpha_\mu x_\mu(\omega) = \gamma(\omega)q(\omega) - f(\omega), \qquad \text{(D.6)}$$

where

$$\gamma(\omega) = \sum_\mu \frac{\alpha^2_\mu}{m_\mu\big(\omega^2_\mu - \omega^2 - i\omega\eta_\mu\big)} \qquad \text{(D.7)}$$

and

$$f(\omega) = \sum_\mu \frac{\alpha_\mu f_\mu(\omega)}{m_\mu\big(\omega^2_\mu - \omega^2 - i\omega\eta_\mu\big)} \qquad \text{(D.8)}$$

Using (D.1) and (D.6) gives

$$-m\omega^2 q(\omega) + \gamma(\omega)q(\omega) = f(\omega). \qquad \text{(D.9)}$$

Using (D.8), (D.7) and (D.5) it is easy to show that

$$\langle f(\omega)f(\omega')\rangle = -\frac{k_\mathrm{B}T}{\pi\omega}\,\mathrm{Im}\,\gamma(\omega)\delta(\omega+\omega'). \qquad \text{(D.10)}$$

Note also that (D.9) is equivalent to

$$m\ddot{q} + \int_{-\infty}^t \mathrm{d}t'\,\gamma(t-t')q(t') = f(t).$$

In Section 3 we studied a system of many coupled dynamical variables

$$m\ddot{q}_i + \int_{-\infty}^t \mathrm{d}t'\,\gamma_{ij}(t-t')q_j(t') = f_i(t)$$

but this problem can be reduced to the problem studied above by forming new dynamical variables, as linear combination of the old dynamical variables q_i, chosen so that γ_{ij} becomes diagonal.

References

1. D.F. Moore, *The Friction and Lubrication of Elastomers* (Pergamon, Oxford, 1972).
2. B.N.J. Persson, *Sliding Friction: Physical Principles and Application*, 2nd ed. (Springer, Heidelberg, 2000).
3. B.N.J. Persson, J. Chem. Phys. **115**, 3840 (2001).
4. B.N.J. Persson, A.I. Volokitin, Phys. Rev. B **65**, 134106 (2002).
5. M. Klüppel, G. Heinrich, Rubber Chem. Technol. **73**, 578 (2000).
6. A. Schallamach, Wear **6**, 375 (1963).
7. Y.B. Chernyak, A.I. Leonov, Wear **108**, 105 (1986).

8. A.E. Filippov, J. Klafter, M. Urbakh, Phys. Rev. Lett. **92**, 135503 (2004).
9. Weak absorption systems (*e.g.*, saturated hydrocarbon molecules or noble-gas atoms on metal surfaces) exhibit extremely low (pinning) barriers for parallel motion. The barriers can be estimated from the measured frequencies of parallel adsorbate vibrations, see. *e.g.*, B.N.J. Persson, Surf. Sci. Rep. **15**, 1 (1990).
10. M.L. Williams, R.F. Landel, J.D. Ferry, J. Am. Chem. Soc. **77**, 3701 (1955).
11. B.N.J. Persson, Phys. Rev. B **51**, 13568 (1995).
12. B.N.J. Persson, O. Albohr, G. Heinrich, H. Ueba, J. Phys. Condens. Matter **17**, R1071 (2005).
13. B.N.J. Persson, E. Brener, Phys. Rev. E **71**, 036123 (2005).
14. B.N.J. Persson, Surf. Sci. **401**, 445 (1998).
15. A. Schallamach, Wear **17**, 301 (1971).
16. A.D. Roberts, A.G. Thomas, Wear **33**, 45 (1975).
17. K. Vorvolakos, M.K. Chaudhury, Langmuir **19**, 6778 (2003).
18. U. Tartaglino, V.N. Samoilov, B.N.J. Persson, J. Phys. Condens. Matter **18**, 4143 (2006).
19. B.N.J. Persson, Surf. Sci. Rep. **61**, 201 (2006).
20. B.N.J. Persson, Phys. Rev. B **63**, 104101 (2001).
21. B.N.J. Persson, J. Phys. Condens. Matter. **18**, 7789 (2006).
22. The force acting on a stress domain should depend quasi-periodically on the lateral displacement x *i.e.*, $F = F_c \sin(2\pi x/a)$ giving for small x: $F \approx F_c 2\pi x/a$. The pinning stress $F_c = \sigma_c D^2$ and the elastic force $F = kx$ with $k = \alpha ED$, where α is of order ~ 6. Thus we get $ED \approx \sigma_c D^2/a$.
23. A. Le Gal, M. Klüppel, J. Chem. Phys. **123**, 014704 (2005).
24. K.A. Grosch, Proc. R. Soc. London, Ser. A **274**, 21 (1963); K.A. Grosch, in *The Physics of Tire Traction: Theory and Experiment*, edited by D.F. Hays, A.L. Browne (Plenum Press, New York, London, 1974) p. 143.
25. A. Casoli, M. Brendle, J. Schultz, A. Philippe, G. Reiter, Langmuir **17**, 388 (2001).
26. T. Baumberger, C. Caroli, Adv. Phys. **55**, 279 (2006); T. Baumberger, C. Caroli, O. Ronsin, Eur. Phys. J. E **11**, 85 (2003); O. Ronsin, K.L. Coeyrehourcq, Proc. R. Soc. London, Series A **457**, 1277 (2001).
27. M.R. Mofidi, E. Kassfeldt, B. Prakash, to be published in Wear.
28. J. Molter, *Elastomerreibung und Kontactmechanik, DIK fortbildungsseminar, Hannover 2003.*
29. D. Forster, *Hydrodynamic Fluctuations, Broken Symmetry, and Correlation Functions* (Benjamin, London, 1975).